Materials and Design 116 (2017) 127–135

Contents lists available at ScienceDirect

Materials and Design

journal homepage: www.elsevier.com/locate/matdes

Composition effects on the fcc-hcp martensitic transformation and on the magnetic ordering of the fcc structure in Fe-Mn-Cr alloys

L.M. Guerrero, P. La Roca, F. Malamud, A. Baruj *, M. Sade

Centro Atómico Bariloche (CNEA), Instituto Balseiro (U.N. Cuyo – CNEA), Av. Bustillo 9500, 8400 Bariloche, Argentina
CONICET, Argentina

HIGHLIGHTS

- The effect of Mn and Cr on T_N of fcc was analyzed.
- The effect of Mn and Cr on the fcc-hcp transformation temperatures was measured.
- Phenomenological models are presented to describe composition effects.

GRAPHICAL ABSTRACT

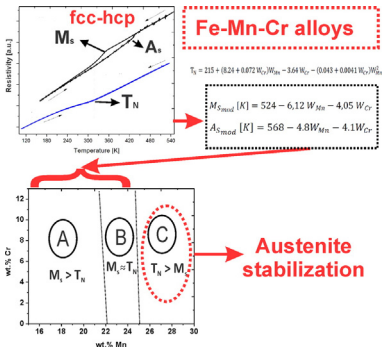

ARTICLE INFO

Article history:
Received 12 September 2016
Received in revised form 21 November 2016
Accepted 1 December 2016
Available online 3 December 2016

Keywords:
Fe-Mn-Cr alloys
Martensitic transformation
Magnetic ordering
Shape memory alloys

ABSTRACT

This paper presents an experimental study on the fcc/hcp martensitic transformation temperatures (MTTs) and Néel temperatures (T_N) of the fcc phase of Fe-Mn-Cr alloys. A wide range of chemical compositions ($13.7 < Mn < 27.5$ wt.% and $0 < Cr < 12.4$ wt.%) has been studied. X-ray diffraction measurements were conducted in order to confirm that the martensitic transformation takes place between an fcc structure and the hcp martensite. Transition temperatures were measured by means of electrical resistivity and dilatometry. All transition temperatures tend to decrease with the increment in Cr content while the addition of Mn decreases the MTTs and increases T_N. These different effects and the stabilization effect of the antiferromagnetic ordering on the fcc austenite result in different MTTs behaviors depending on whether the martensitic transition occurs from a magnetically ordered austenite or not. For these later cases, a phenomenological model of MTTs is presented that could be of use for alloys design.

1. Introduction

Fe-Mn-Cr alloys have been the subject of numerous studies for several reasons. During Ni-shortage periods, like those produced by policy decisions on war times, Mn has been regarded as a viable low-cost replacement for Ni in austenitic steels. High Mn additions, typically between 20 wt.% and 40 wt.%, have the effect of stabilizing the fcc austenite (γ), even at very low temperatures [1], suppressing the ferromagnetic transition associated to the bcc martensitic phase (α'). This stabilization is related to the antiferromagnetic ordering of γ, which effectively increases its relative phase stability in comparison to the competing α' and hcp (ε) phases [2,3]. These antiferromagnetic steels, sometimes dubbed as "non-magnetic", have excellent mechanical properties under cryogenic conditions [4], resulting useful for

* Corresponding author at: Centro Atómico Bariloche (CNEA), Instituto Balseiro (U.N. Cuyo – CNEA), Av. Bustillo 9500, 8400 Bariloche, Argentina.
E-mail address: baruj@cab.cnea.gov.ar (A. Baruj).

http://dx.doi.org/10.1016/j.matdes.2016.12.003
0264-1275/

constructing the supporting structure of superconductor magnets. Later on, Fe-Mn-Cr steels found their way into nuclear facilities design due to their lower neutron activation properties in comparison to Ni-containing steels [5]. Thanks to these cryogenic and radiation-related properties, complex multicomponent alloys based on the Fe-Mn-Cr system are being considered as structural materials in fusion reactors. Specifically, Fe-Mn-Cr-based alloys are potential candidates for the manufacture of superconducting magnets in the ITER prototype of fusion nuclear reactor [6].

Another reason of interest in Fe-Mn-Cr alloys is related to their ability to absorb deformation through stress-induced martensitic transformations [7]. Quenched Fe-Mn-Cr alloys containing between 15 wt.% and 30 wt.% Mn undergo a γ to ε martensitic transformation, either by cooling or by applying mechanical forces [8,9]. For smaller amounts of Mn both ε and α' martensites might form. In all these cases, the γ-ε transformation involves the movement of crystalline interphases, a dissipative process useful for damping applications [10]. This capacity to dissipate energy, i.e. elasto-plastic damping, in addition to good mechanical properties as high ductility and mechanical resistance has led to an increased interest on high Mn Fe-Mn based alloys in general [11–17] and the so-called TWIP/TRIP Fe-Mn-Cr alloys in particular [7,9,18]

Despite these promising possibilities from the point of view of practical applications, knowledge is still lacking concerning the relative phase stability between γ and ε in Fe-Mn-Cr alloys. As it is the case in the parent Fe-Mn system, the fcc structure of Fe-Mn-Cr alloys can be retained by quenching from high temperature. The hcp martensite is metastable and forms from the fcc phase either thermally induced by cooling or by applying mechanical stress. Additionally, the stability of the fcc austenite increases if the para- to antiferromagnetic transition takes place, which might inhibit the fcc to hcp transition either partially or completely. Up to now, only a few works have reported experimental data on the structural and magnetic transitions of Fe-Mn-Cr alloys [7,8,19–21]. The aim of the present manuscript is to present a systematic experimental study on the critical temperatures in a wide range of Mn and Cr compositions. In this way, relevant information is presented that is required for deeper analysis on the γ/ε relative phase stability in Fe-Mn-Cr and in Fe-Mn-Cr-based alloys.

2. Experimental

Fe-Mn-Cr alloys were prepared from commercially pure metals (99.9 Fe, 99.9 Mn and 99.9 Cr) by arc melting several times under Ar atmosphere. The resulting alloys (buttons of approximately 15 g) were heat-treated in quartz capsules under Ar atmosphere for 48 h at 1273 K. The buttons were afterwards water quenched by breaking the capsules. Samples for electrical resistivity (1 mm × 3 mm × 20 mm) and dilatometry (3 mm × 3 mm × 12 mm) measurements were cut by spark-erosion from the buttons. All samples were polished, individually encapsulated into quartz tubes under Ar atmosphere, annealed for 1 h at 1273 K, and water quenched by breaking the capsules.

The chemical composition for each alloy studied in this work was determined using the neutron activation technique in the RA-6 experimental reactor at Centro Atómico Bariloche [2]. Table 1 summarizes the results of the compositional analysis. The alloys are named using capital letters and are presented according to an increasing amount of Mn content. Most of the transformation temperatures were determined by using an electrical resistivity equipment that uses a current of 100 mA. In some selected cases supplementary dilatometry measurements were performed using a home-made dilatometer in order to identify a certain phase transformation [2]. In all cases, a spot welded Chromel-Alumel thermocouple was placed on the surface of the corresponding samples in order to accurately measure the temperature. Measurements were performed at cooling or heating rates equal or lower than 5 K/min. More details concerning electrical resistivity and dilatometry measurement applied to Fe-Mn-based alloys have already been reported in the literature [22]. The grain size of the austenite was measured in several samples by applying the intercept line method obtaining average values between 500 μm and 900 μm. In order to confirm the structure of the austenite and formed martensites X-ray measurements have been performed at room temperature (RT), using a Bruker D8 Advance diffractometer. The diffractometer has a Cu anode, monochromator and a Lynx Eye line detector.

Table 1
Composition of the used alloys, determined by neutron activation analysis.

Alloys	Wt.% Fe (±0.9%)	Wt.% Mn (±0.4%)	Wt.% Cr (±0.1%)
A	83.7	13.7	2.6
B	72.9	16.7	10.4
C	71.0	17.1	11.9
D	76.6	17.3	6.1
E	79.3	17.9	2.8
F	70.8	19.1	10.1
G	68.3	19.6	12.1
H	74.1	19.7	6.2
I	69.6	19.7	10.7
J	70.0	19.8	10.2
K	73.8	20.0	6.2
L	76.6	20.7	2.7
M	76.8	20.7	2.5
N	66.6	21.0	12.4
O	67.7	21.9	10.3
P	66.4	22.9	10.7
Q	65.6	24.3	10.1
R	73.2	24.7	2.1
S	69.1	24.9	6.0
T	60.5	27.1	12.3
U	66.3	27.5	6.1

3. Results

3.1. Description of measurements

Martensitic transformation temperatures (M_S, M_f, A_s and A_f) as well as the antiferromagnetic ordering temperatures of the fcc structure (T_N) have been measured. M_s and A_s are defined as the critical temperatures to start the fcc-hcp and the hcp-fcc martensitic transitions respectively. M_f and A_f are the temperatures where no further changes related to each structural transition can be detected [22]. Electrical resistivity is suitable to detect martensitic transitions in Fe-Mn-based alloys [22,23]. In particular, Fe-Mn-Cr samples show a decrease in the electrical resistivity during the γ to ε transformation and an increase during the reverse transformation. In addition, the martensitic transition is characterized by the presence of a thermal hysteresis if both, the direct and reverse transitions are measured.

On cooling, the para- to antiferromagnetic transition of the austenite can be detected by a change in the slope of the electrical resistivity curve, as it has been used to study Fe-Mn alloys and several other materials [20,24]. A nice example of the application of this technique is in the case of the antiferromagnetic ordering transition that takes place in pure Cr [25]. An useful way to discern between the magnetic ordering and structural transitions in Fe-Mn alloys is that no thermal hysteresis in electrical resistivity measurements is associated to the former [20].

In order to present and analyze the results it is convenient to consider that the temperature for magnetic ordering depends on the alloy chemical composition, while martensitic transformation temperatures might also depend on other factors such the performed thermal treatments and alloy microstructure. Additionally, martensitic transformation temperatures might be strongly affected by the magnetic state of the austenite [22,23]. Therefore, electrical resistivity measurements can result in different characteristic behaviors, which are shown in Fig.1a.

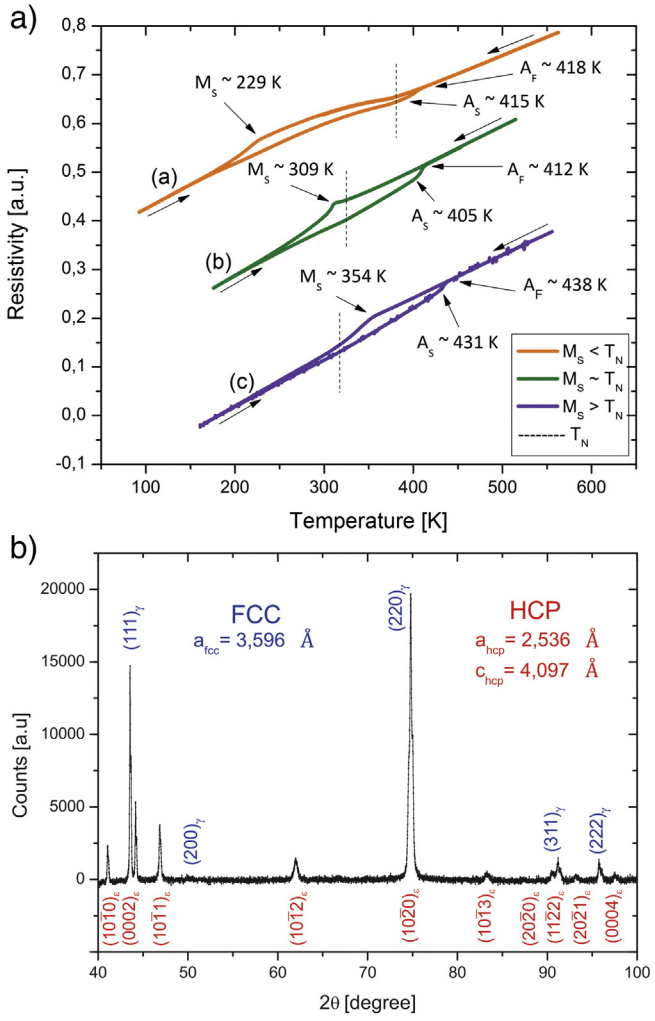

Fig. 1. a) Electrical resistivity vs. temperature measurements for selected Fe-Mn-Cr alloys. Curve (a) was obtained for alloy U corresponding to $M_s < T_N$. Curve (b) was obtained for alloy P and corresponds to the case where M_S is close to T_N. Curve (c) was obtained for alloy I and shows the case for $M_S > T_N$, where the magnetic ordering is masked by the martensitic transformation. b) X-ray diffractogram of alloy K where fcc and hcp peaks are indentified.

In this Figure, electrical resistivity measurements for 3 different alloys are presented: curve (a) $T_N > M_s$ (alloy U), curve (b) T_N close to M_s (alloy P) and curve (c) $T_N < M_s$ (alloy I). Curve (a) shows that structural and magnetic transitions are readily detected on cooling and heating if T_N is sufficiently higher than M_s. In the case of curve (b), where T_N is slightly higher than M_s, both transitions can be detected during cooling. However, the magnetic ordering of the austenite can only be observed for a small temperature range, which makes the precise measurement of T_N rather difficult. Finally, curve (c) is an example of those cases where the magnetic ordering of the remaining γ phase cannot be easily detected. The difficulty arises due to the strong resisitivity variation produced by the γ to ε martensitic transformation and due to the fact that the magnetic ordering resistivity variation will depend on the amount of remaning austenite. In order to clarify this point, an X-ray diffractogram of sample K is presented in Fig. 1b. The analysis of the obtained peaks shows that the martensitic transformation takes place between an fcc structure and the hcp martensite. Furthermore, remaining austenite is still present at room temperature (which is well below M_s). It has been verified that X-ray analysis performed at room temperature (RT) on samples previously cooled down well below M_f (with As > RT) also show retained austenite.

As it was shown in Fig. 1a, the magnetic transition might not not be easily measured (curve (b)) or could even be completely undetectable (curve (c)). Under such conditions, a procedure to avoid the γ to ε transformation was applied. It consisted on hot rolling the samples at a temperature higher than M_d, i.e. the limit temperature at which martensite can be stress induced [26]. In this way, only plastic deformation of the austenite takes place during rolling and a large density of crystalline defects is introduced in the fcc phase, which effectively suppresses the martensitic transformation [27]. Once the martensitic transition is suppresed, a well detectable change of slope in the electrical resistivity measurement can be observed enabling the accurate measurement of T_N. An example of the results obtained with this procedure is shown in Fig. 2a, where measurements for alloys I (curves (a) and (b)) and U (curves (c) and (d)) are presented in both states: before and after hot rolling. In curves (b) and (d), no hysteresis is obtained as expected when only the magnetic transition takes place. It's interesting to notice that in the curve (c) it is possible to determine T_N during cooling and it coincides with the value obtained in the "after rolling" condition (curve (d)). This result shows that the plastic deformation introduced after hot rolling the sample does not affect the T_N value.

It is worth mentioning that in order to emphasize the quality of the measurements of the martensitic transformation temperatures (M_s and A_s), dilatometry measurements were performed on several samples. In

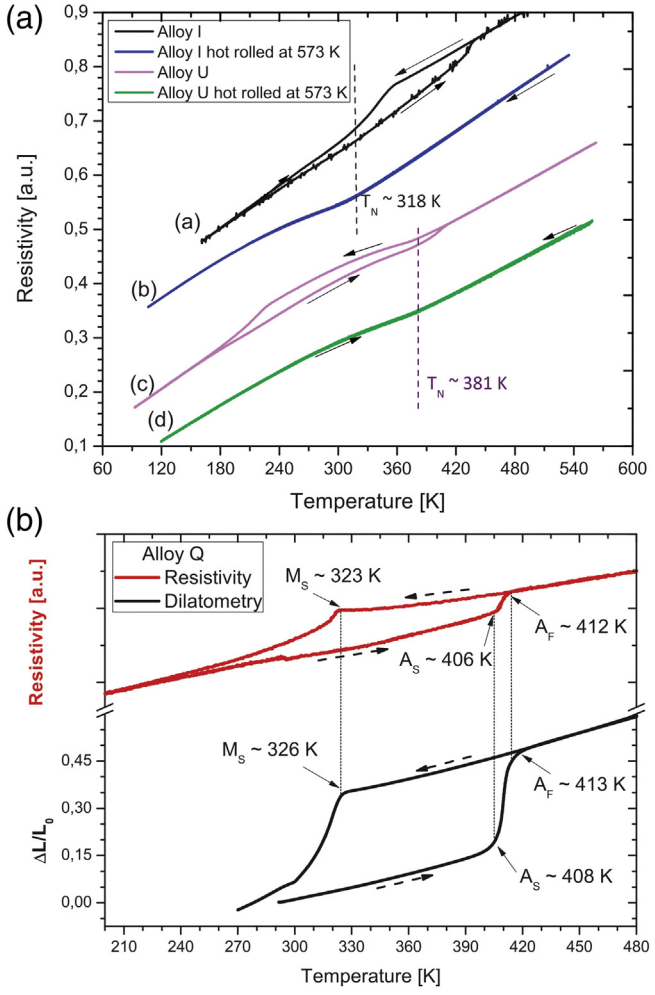

Fig. 2. a) Electrical resistivity vs temperature measurements for alloys I and U. Curves (a) and (c) correspond to samples I and U after normal thermal treatment and curve s (b) and (d) correspond to samples hot rolled at 573 K. In these latter cases the martensitic transition is suppressed and the magnetic transition is the only one observed. b) Comparative analysis of resistivity and dilatometric measurements for alloy Q.

Fig. 2b, an example is presented. Transformation temperature values obtained with both techniques were found to be consistent. It is interesting to consider that at temperatures below M_f, some austenite is still present in the measured samples. This implies that during heating of the samples, if $T_N < A_f$, it would also be possible to obtain data on T_N, by detecting changes in the slope of the electrical resistivity curves which will vary depending on the fraction of remaining austenite. This can be observed in curve (b)) in Fig.1a and in curve a) of Fig.2a. On one hand it is clear that the measurement of T_N when no martensite is present, or when T_N is sufficiently higher than M_s., will make it easier to obtain accurate results. On the other hand it is noticed that the existence of remaining austenite at $T < M_f$ enables to obtain T_N when the partially transformed sample is heated, method which has been used in several samples. Moreover, it has been confirmed in alloys D and I that T_N obtained from the slope change of the resistivity curve during heating, of a sample previously cooled down to $T < M_f$, leads to the same value as the one obtained from an austenitic sample previously hot rolled at $T > M_d$. It is clear then that plastic deformation of austenite does not alter the temperature for the para to antiferromagnetic transition as it is expected.

An additional case deserves some attention. In a few samples, the measurement of A_s by means of electrical resistivity is difficult since changes in the slope of the curves are small or even negligible. An example of this situation can be observed in Fig. 3 for alloy U where the hcp-fcc transformation takes place in the same temperature range where the magnetic disordering transition of fcc takes place. In this case A_s was determined by the measurement of thermal expansion, where a clear step in the heating curve (see Fig. 3b) is apparent as a consequence of the volume change between both structures. This alloy shows another interesting behavior which is to be noticed. A second transformation cycle (see curve red in Fig. 3a) shows no fcc-hcp transformation, phenomenon which is also present in alloy T, i.e., in those alloys where Mn content is the largest among the Mn range analyzed in the present work (Mn content >27 wt.%). This phenomenon can be rationalized considering a strong stabilization of the fcc phase due to the antiferromagnetic ordering transition. Although a detailed analysis of the effects of thermal cycling through the martensitic transformation is out of the scope of the present manuscript, previous results have shown a similar result in an alloy with a close composition [9,21]. Moreover, it has been shown in Fe-Mn-Si alloys that for temperatures below T_N the effect of magnetic ordering on the Gibbs free energies inhibit the increase of the driving force leading to a strong inhibition of hcp formation.

Alloy A (13.7 wt.% Mn, 2.6 wt.% Cr) has the smallest Mn content among the studied alloys. The electrical resistivity curve (Fig. 4a) shows a very small hysteresis which might correspond to the fcc-hcp cycle. However, only M_f and A_f could be obtained from this measurement. In order to determine M_s. and A_s, a dilatometry measurement is suitable here being shown the obtained curve in Fig. 4b. It can be expected from reported results on Fe-Mn alloys that the bcc martensite will be present for this composition [2]. However, it was reported for a binary alloy with the same amount of Mn that a small amount of hcp martensite is also formed. The visible contraction observed during cooling and expansion during the heating curve can be reasonably explained by the existence of small amount of hcp formation and its retransformation to austenite. Moreover, the obtained M_s. and A_s values differ from the reported ones for the binary alloy following the same trend as the observed one for the effect of Cr on these temperatures as explained below. Additionally, the formation of bcc martensite is also observed in Fig. 4b by a well detectable expansion during cooling which is also indicated in the figure.

3.2. Critical transformations temperatures

The obtained fcc-hcp martensitic transformation temperatures and Néel temperatures of the fcc phase are listed in Table 2. It is also indicated in which cases T_N was measured in hot rolled specimens. It should be mentioned that in most of the measured samples, M_s. is higher than room temperature which indicates that the obtained values correspond to the second fcc-hcp transformation after the thermal treatment at 1273 K, while the reported A_s temperatures correspond to the first reverse transformation after the thermal treatment.

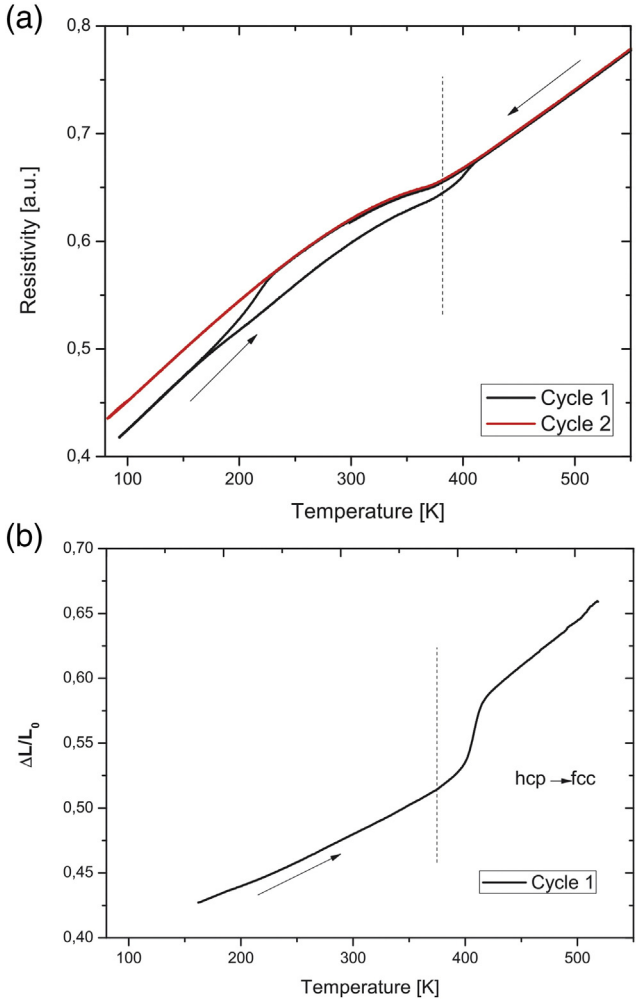

Fig. 3. a) Electrical resistivity measurement for alloy U (27.5 wt.% Mn and 6.1 wt.% Cr). In the second cycle (red curve) the martensitic transition is suppressed and only the magnetic transition is observed. b) Dilatometry measurement for the same alloy, where expansion corresponding to hcp-fcc retransformation is indicated. (For interpretation of the references to colour in this figure legend, the reader is referred to the web version of this article.)

The obtained magnetic ordering and martensitic transformation temperatures are shown in Figs. 5, 6 and 7 as a function of composition. In these figures each data point represents the composition of one of the measured alloys, and the number close to it is the measured T_N (Fig. 5), M_S (Fig. 6) or A_S temperatures, in K (Fig. 7). The x-axis of these figures corresponds to the Mn content of the alloys, while the Cr content is indicated in the y-axis.

From Fig. 5 it can be noticed that in alloys containing similar Cr contents, T_N increases as Mn content increases, while at constant Mn content, T_N decreases as the Cr content increases. So, Cr and Mn affect the behavior of the T_N in different ways, while Mn tends to reinforce magnetism, Cr shows a weakening effect. From Figs. 6 and 7 it can be observed that M_s. and A_s temperatures decrease as either Mn or Cr content increases.

4. Discussion

From the obtained results it is noticed that the Néel temperature of the fcc structure is determined by the composition of the alloy as it is

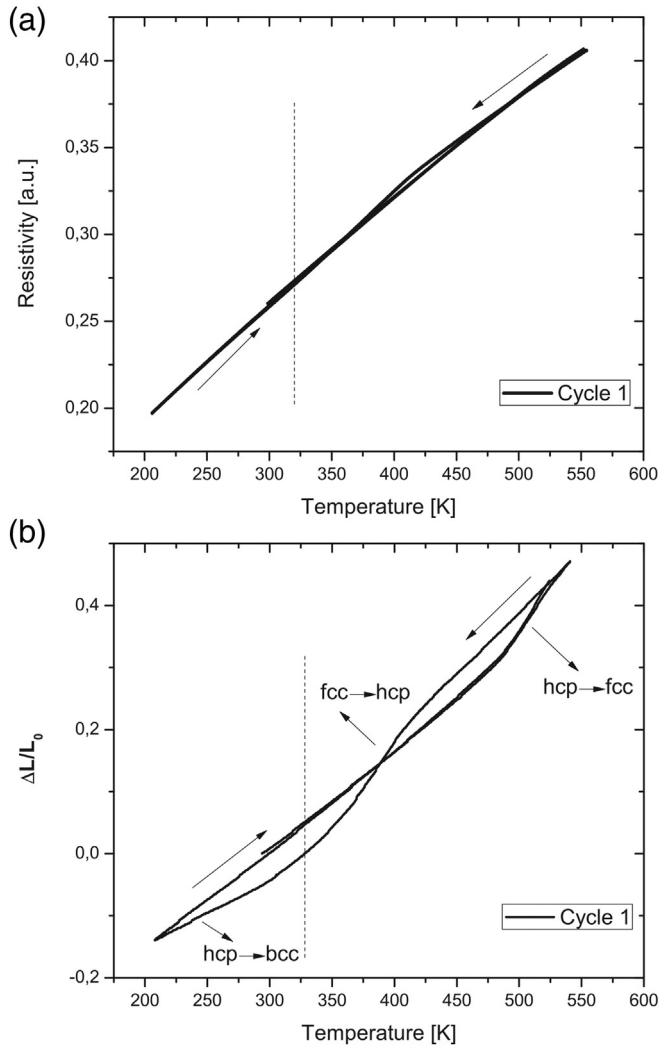

Fig. 4. a) Electrical resistivity measurement for alloy A (13.7 wt.% Mn and 2.6 wt.% Cr). b) Dilatometry measurement for the same alloy, where contraction and expansion corresponding to fcc-hcp formation and hcp-fcc retransformation are indicated. The slope change related to the formation of bcc martensite is also indicated.

expected from previous results in binary Fe-Mn and Fe-Mn-Si alloys. On the other hand, a completely different situation arises if the martensitic transformation temperatures are considered. In fact the magnetic ordering of the fcc phase clearly affects the martensitic transformation. This fact stresses the need to predict the Néel temperatures as a function of the composition of the alloy if the martensitic transition is to be controlled. In the following we will analyze possible phenomenological modeling of the critical temperatures.

4.1. Modeling T_N temperatures

The present results clearly indicate that T_N increases if the content of Mn increases and/or if the Cr content decreases. Additionally, we have focused our experimental study in the composition range where the fcc-hcp martensitic transformation takes place. Additional data on the magnetic ordering of the austenitic structure in Fe-Mn-Cr alloys has been presented by Khomenko et al. [19] who reported measurements of T_N for Mn contents starting from 22 wt.% and up to 40 wt.%. It is noticed that in Ref. [19] T_N values were obtained for 0, 4 and 10 wt.% Cr, while in the present manuscript several alloys with approximately 6, 10 and 12 wt.% Cr have been measured, starting from 13.7 wt.% Mn. This similarity gives an excellent opportunity to compare

Table 2
Measured martensitic transformation temperatures M_s, A_s, M_f, A_f and magnetic ordering temperature of the fcc structure (T_N). Symbol (•) indicates those samples where T_N was measured after hot rooling at T > Md. Values obtained by means of dilatometry measurements are indicated by symbol (*). Results obtained from phenomenological models are also included (T_N mod and M_s mod).

Alloys	T_N exp. [K]	T_N mod [K]	M_s [K]	M_f [K]	A_s [K]	A_f [K]	M_s mod [K]
A	–	310.7	411(*)	–	488(*)	529(*)	426.7
B	302	303.7	371	250	445	462	376.6
C	301	300.5	367	218	435	440	368.4
D	311(•)	322.8	401	296	463	470	390.5
E	330	338.9	396	185	465	481	400
F	322	318.7	364	218	432	440	363.2
G	304	314.1	353	170	421	428	351.9
H	345	336.9	378	161	455	476	375.3
I	318(•)	320.1	354	214	431	438	357.1
J	326	321.9	368	200	431	437	358.5
K	347	338.7	385	224	449	455	373.6
L	351	356.8	372	251	453	464	383.5
M	369	356.9	395	201	457	478	384.4
N	311	320.1	340	148	416	427	342.3
O	329	333.5	342	231	418	423	344.9
P	325	336.6	309	216	405	412	337.5
Q	341	346.1	323	194	406	412	331.2
R	384	383.1	376	264	446	459	361.3
S	371	367	361	200	437	444	344.4
T	336	349	277	181	377	383	305
U	381	380.0	229	145	415(*)	418	327.6

measurements of alloys with close compositions and to suggest a phenomenological model for a large range of compositions.

Considering results presented in Ref. [19] and in the present manuscript, a linear dependence is not suitable to fit the obtained dependence of T_N on Mn or Cr content (see Fig. 8). Therefore a quadratic dependence on Mn content was proposed, where the coefficients depend linearly on the amount of Cr. This is because it was observed that the T_N vs. Mn functional shape is strongly affected by Cr content as it can be seen in Fig. 8. Taking into account the whole set of data originated in both works, the following equation is proposed to describe the effect of composition on T_N, where Mn and Cr contents are in expressed in wt.%:

$$T_N = 215 + (8.24 + 0.072\,W_{Cr})W_{Mn} - 3.64\,W_{Cr} - (0.043 + 0.0041\,W_{Cr})W_{Mn}^2 \quad (1)$$

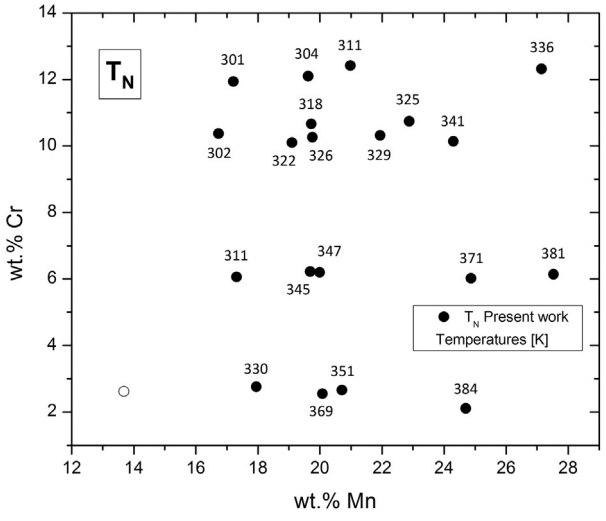

Fig. 5. Measured Néel temperature (T_N) of the metastable fcc structure (austenite) obtained for the Fe-Mn-Cr alloys studied in the present work (circles). The empty circle indicates the additional presence of bcc martensite (α'); T_N was not detected for this alloy. Temperatures are indicated in K.

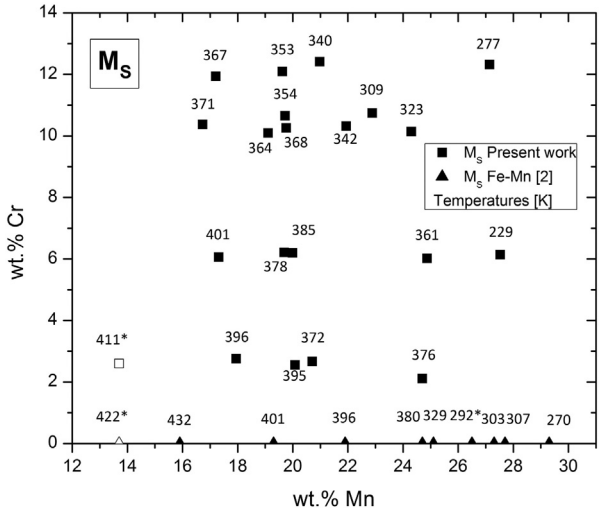

Fig. 6. $M_{s.}$ temperatures corresponding to the fcc-hcp martensitic transformation obtained in the present work for each of the measured compositions (square symbols). $M_{s.}$ values determined in Ref. [2] for Fe-Mn binary alloys are also shown (triangles). Temperatures in K. Dilatometry results are indicated by the symbol * and empty symbols indicate the presence of α' martensite (bcc).

where W_{Mn}, W_{Cr} describe the content of Mn and Cr in wt.%, respectively. Fig. 8 shows the experimental data of T_N vs. Mn content obtained in the present manuscript and the reported by Khomenko et al. In particular, a good agreement between data from [19] and the present work can be observed for 10 wt.% Cr, where data from both sources can be directly compared. Additionally, the curves corresponding to Eq. (1) are plotted considering Cr content as a fixed parameter (0, 4, 6.5, 10.4 and 12.5 wt.% Cr). The data are well described by Eq. (1). The proposed model correctly describes magnetic ordering temperatures for Mn contents starting at 17 wt.% and up to 40 wt.%, and Cr content up to 12 wt.%. In this figure, data for 0 wt.% Cr (i.e., Fe-Mn alloys) reported by Khomenko et al. are included. These data are also fitted adequately by Eq. (1), which implies that the proposed model for the ternary alloys reasonably extrapolate to the Fe-Mn binary system. The present phenomenological model shows an excellent agreement with the model presented by Huang for the binary Fe-Mn alloys, in the composition range starting from 24 wt.% [28]. For binary alloys with Mn contents

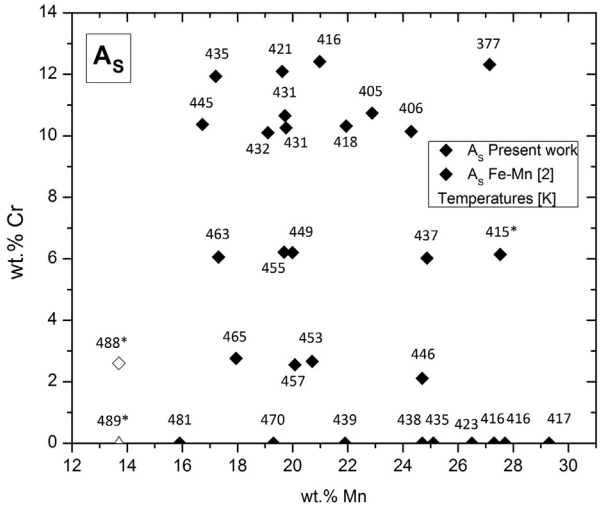

Fig. 7. A_s temperatures corresponding to the hcp-fcc transformation obtained in the present work for each composition (diamond solid symbols). Values obtained for the binary Fe-Mn alloys in Ref. [2] are also shown (triangle symbols). The empty symbols (diamonds and triangles) indicate the presence of bcc martensite. Symbol * corresponds to results obtained by dilatometry measurements.

smaller than 24 wt.%, the model presented in Ref. [28] for binary alloys shows some discrepancy with the plot of Eq. (1) and an experimental point obtained by [19]. However, the available data on T_N for alloys with Mn contents smaller than 20 wt.% are scarce; an aspect that requires further experiments for a deeper analysis and does not alter the present results.

Eq. (1) differs from the linear description presented by Zhang et al. [20] for Fe-Mn-Al-Cr-C alloys, where the effect of each component is set as a linear term independent of the contribution of the other elements. It is convenient to remark that in the cited manuscript [20], the effect of Cr and Mn are obtained from measurements performed in alloys with a higher amount of components (adding Al and C), being the composition range of Mn and Cr narrower than the one presented here. Considering those measurements obtained for Mn contents smaller than 25 wt.% (Fig. 8) it might be possible to fit the experimental data by a linear function, with coefficients of the order of those reported in [20]. If larger amounts of Mn are taken into consideration, the results obtained by Khomenko et al. and in the present manuscript on T_N cannot be described by a linear function of Mn and Cr contents.

In order to emphasize the good agreement found between the proposed effect of Mn and Cr contents on T_N and the data from [19] a new graph is shown in Fig. 9. There, the experimentally obtained Néel temperatures (T_N exp) are plotted vs. the modeled ones (T_N mod), obtained from Eq. (1). The linear curve corresponds to the relationship $T_{N\,exp.} = T_{N\,mod.}$ It is clear that Eq. (1) can be used to predict temperatures for magnetic ordering of austenite in the present composition range.

4.2. Modeling $M_{s.}$ temperatures

In order to get a closer understanding on the effect of Cr on the critical martensitic transformation temperatures, Fig. 10a shows the effect of Cr on $M_{s.}$ for alloys with a nearly constant Mn content (around 20 wt.% Mn). A linear fit seems to be reasonable for the obtained data. A linear fit is also a good description of the effect of Mn content if Cr is kept fixed for those cases where $T_N < M_{s.}$, as commented below.

Concerning the fcc-hcp martensitic transformation a relatively extended composition range has been experimentally analyzed in the present manuscript. This fact encourages to suggest a model taking in consideration both the effects of Mn and Cr on the martensitic transformation temperatures. A first approximation of the experimental results about the effects of Mn and Cr on M_S temperatures can be modeled by Eq. (2), which is in good agreement with the experimental data as long as $M_S > T_N$.

$$M_{S\,mod}\,[K] = 524 - 6,12\,W_{Mn} - 4,05\,W_{Cr} \quad (2)$$

A phenomenological equation is also suggested for the effect of Mn and Cr contents on A_s:

$$A_{S\,mod}\,[K] = 568 - 4.8W_{Mn} - 4.1W_{Cr} \quad (3)$$

Notably, the coefficients corresponding to Mn content in Eqs. (2) and (3) and the independent terms are very close to those reported by Cotes et al. [2] for Fe-Mn binary alloys as long as $M_S > T_N$. The addition of Cr does not alter the effect of Mn on the martensitic transformation temperatures if the austenite is paramagnetic in the considered composition range.

On the other hand, if the fcc phase becomes antiferromagnetically ordered at a temperature higher than the martensitic transformation temperature, the M_S temperature decreases drastically, away from the model. This situation can be seen in Fig. 10b, where the dotted line corresponds to Eq. (2) and correctly describes the data if $M_{s.} > T_N$. In the same figure, the arrow indicates the experimental data which lies clearly away from the linear behavior, as the fcc becomes antiferromagnetic before transforming to hcp martensite.

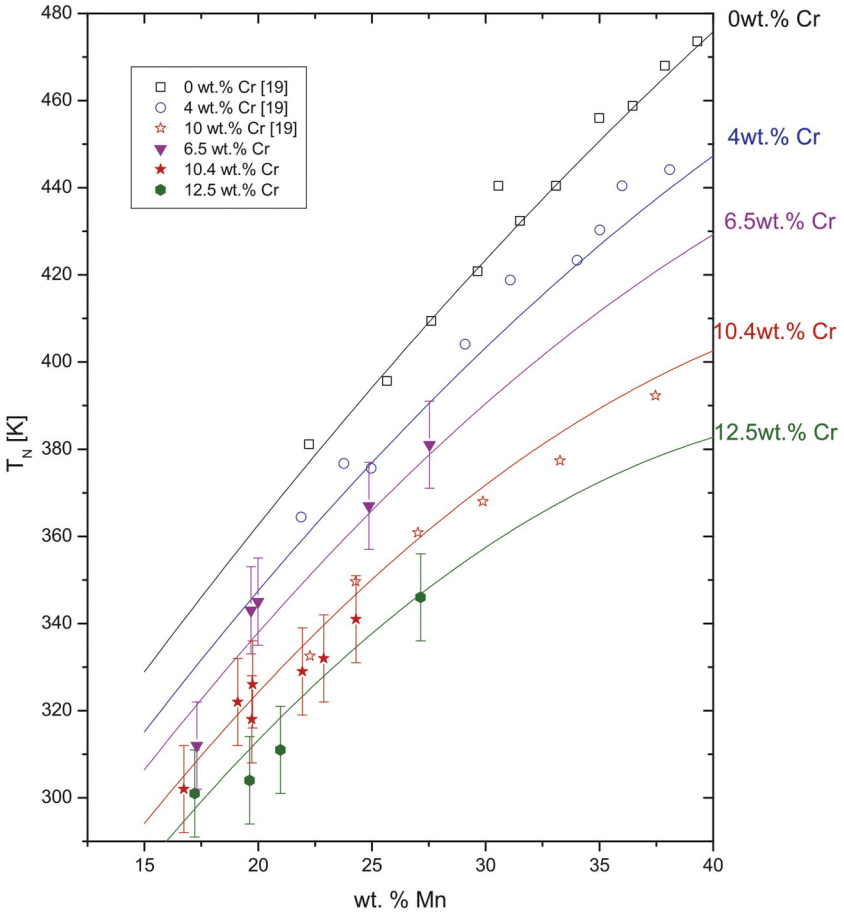

Fig. 8. Néel temperatures vs. Mn content for different amounts of Cr content. Values obtained in this work, and reported by Khomenko et al. [19] are included. T_N measurements of Fe-Mn binary alloys also reported in [19] are included. Curves correspond to the proposed phenomenological model (Eq. (1)).

A significant difference between the effect of Cr if compared with Mn, is that an increase of Cr if Mn content is kept constant, leads to a decrease of both critical temperatures, M_s and T_N. An example for alloys with 24.3 wt.% Mn is shown in Fig. 11. In this case both transitions, the martensitic one and the magnetic ordering of the austenite take place at rather close temperatures. This behavior might be considered as an intermediate stage since larger Mn contents lead to alloys where T_N becomes considerabley larger than M_s while the opposite situation takes place for smaller contents of Mn.

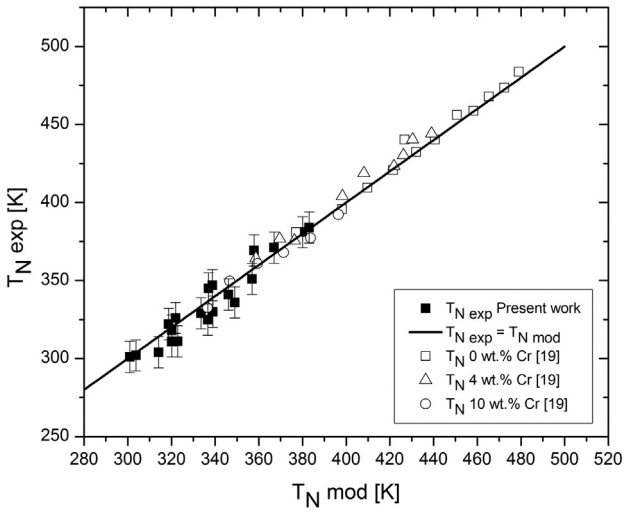

Fig. 9. Experimentally obtained Néel temperatures vs. modeled T_N values. Data for Fe-Mn-Cr alloys obtained in the present manuscript and those for Fe-Mn-Cr and Fe-Mn alloys reported by [19], are also included.

The linear dependence of M_s temperatures as a function of Mn content for a fixed Cr content, and the visible separation from this relationship once T_N becomes larger than M_s, corroborates that magnetic ordering of the austenite stabilizes this phase in comparison with the hcp martensite. A good agreement between all determined M_s and Eq. (2) is noticeable if the experimentally obtained M_s ($M_{s\ exp}$) are plotted vs. the obtained values from Eq. (2) (M_s^{mod}). This is observed in Fig. 12 where the straight line corresponds to $M_s^{exp} = M_s^{mod}$ and all data corresponding to alloys where $T_N < M_s$ fall close to the linear curve while those experimental data where $T_N > M_s$, clearly separate from the line. A similar phenomenon was reported for Fe-Mn based alloys, where a strong effect of magnetic ordering on the Gibbs energy of the austenite was found [29,30]. A thermodynamic analysis on the Gibbs energy of the fcc and hcp structures in the Fe-Mn-Cr alloys is still necessary to get a deeper comprehension on the topic. However it can be expected that the driving force of the fcc-hcp transformation will not sufficiently increase once the austenite becomes antiferromagnetic, hampering in this way the formation of the hcp martensite. This relative stabilization of the fcc structure may lead to an increase of the technological interest since several applications require to have a non ferromagnetic phase down to cryogenic temperatures, keeping good mechanical properties [4].

Finally, it can be mentioned that Cr plays several roles in Fe-based alloys. It is usually used to increase corrosion resistance in steels, in additions over 6.7 wt.%. Its structural effect is mainly to stabilize the ferritic phase. On the other hand, if Cr content is higher than 20 wt.%, a tetragonal phase (σ) precipitates at high temperatures, which increases alloy brittleness. This effect can be neutralized by the addition of Ni, which increases the fcc stability. Controlling Cr and Ni additions, either ferritic or

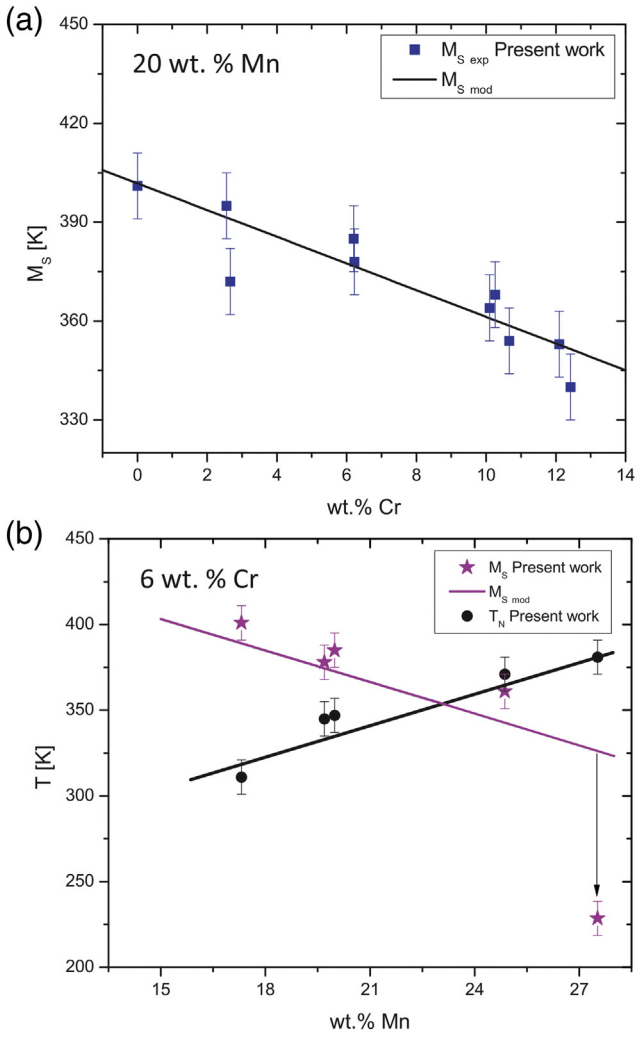

Fig. 10. a) Measured $M_{s.}$ transformation temperatures (fcc-hcp) vs. Cr content for alloys with Mn content approximately equal to 20 wt.%. and $T_N < M_s$. The line corresponding to Eq. (2) is also plotted. b) Measured $M_{s.}$ and T_N values for several alloys with 6 wt.% Cr content vs. Mn content. As T_N becomes higher than $M_{s.}$, the linear fit corresponding to Eq. (2) does not describe any more the obtained behavior.

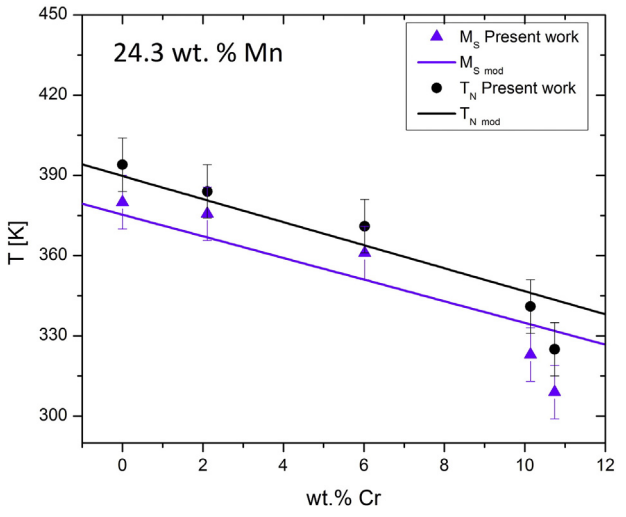

Fig. 11. Ms. temperatures for the fcc-hcp martensitic transformation and Néel temperature (T_N) of the fcc phase vs. Cr content for alloys with 24.3 wt.% Mn.

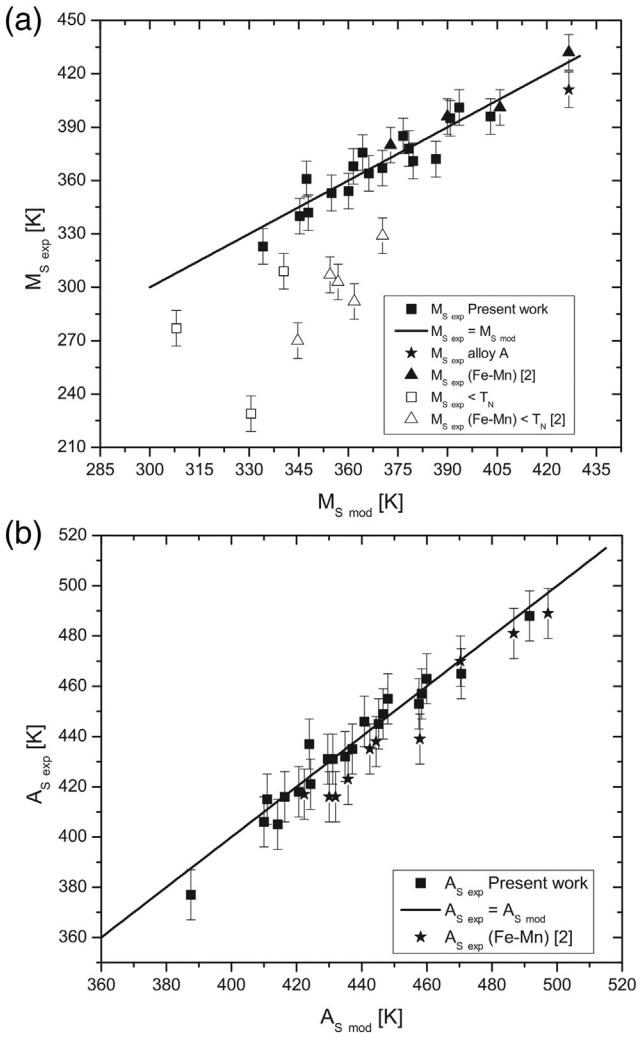

Fig. 12. Experimentally obtained a) $M_{s.}$ and b) A_s temperatures vs. modeled values. Data for Fe-Mn-Cr alloys obtained in the present manuscript and Fe-Mn alloys reported by [2], are also included. The empty symbols in the figure represent the data where $T_N > M_s$.

austenitic steels can be prepared. In the present manuscript two additional specific consequences of adding Cr to Fe-Mn alloys have been carefully studied. On one hand the addition of Cr up to 12 wt.% decreases T_N of the fcc structure, decreasing the stability of this phase. On the other hand adding Cr, $M_{s.}$ for the fcc-hcp transition decreases, which can be considered as a stabilizing effect of the austenite. Both effects, which are opposite if the stabilization of the austenitic structure is considered, add interesting possibilities for controlling $M_{s.}$ temperatures and design of alloys with specific properties, like the shape memory effect. It is clear that the behavior of the alloys concerning the fcc to hcp martensitic transformation will depend on the magnetic state of the austenite. The results reported in the present manuscript allow to present a composition diagram where three regions can be distinguished (Fig. 13): Region A where the martensitic transition starts in a paramagnetic fcc phase, region B where the formation of hcp starts in the antiferromagnetic austenite, and region C where a transition behavior can be found.

The effect of Mn in Fe-Mn-Cr alloys is similar as the role it plays in binary Fe-Mn and ternary Fe-Mn-Si and Fe-Mn-Co alloys. In fact, the addition of Mn stabilizes the fcc austenite decreasing the $M_{s.}$ temperature of the fcc-hcp transformation. The austenite is further stabilized by the increase in the magnetic transition temperature as the Mn content increases. In this way an opposite effect of Mn and Cr on the magnetic transition temperature of the austenite and the similar effect of both

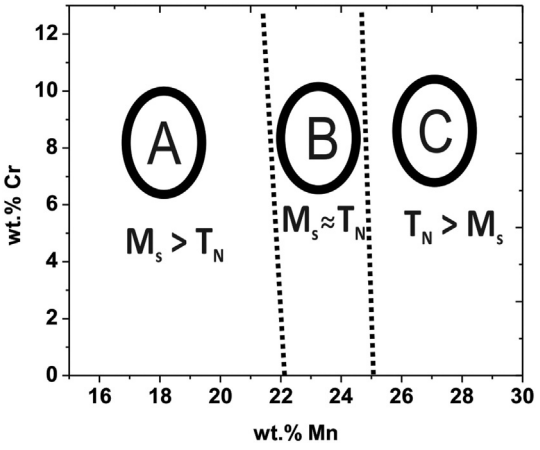

Fig. 13. Schematic composition diagram where different behaviors are found corresponding to: A) $M_s > T_N$, B) M_s close to T_N and C) $M_s < T_N$.

elements on the martensitic transformation temperatures enable to obtain a wide variety of controlled behaviors in the Fe-Mn-Cr system.

5. Conclusions

The effects of Mn and Cr on the fcc-hcp transformation temperatures and on the Néel temperature of the fcc structure of Fe-Mn-Cr alloys have been studied for a wide chemical composition range ($13.7 < Mn < 27.5$ wt.% and $0 < Cr < 12.4$ wt.%). Considering isoMn lines, the addition of Cr has the effect of shifting the martensitic transformation temperatures and the Néel temperature of the austenite to lower values. The increment of Mn content has the effect of increasing T_N and decreasing A_s and M_s. Three different types of behaviors can be identified depending on whether T_N is below, near or above M_s. In the first case, martensitic transformation temperatures show a smooth variation with Mn and Cr addition and can be described using a simple phenomenological model (Eq. (2) and Eq. (3)). In the case where $T_N > M_s$, the antiferromagnetic ordering strongly stabilizes the austenite shifting M_s temperatures to considerably lower values. These alloys show marked differences between the first and second transformation cycles (Fig. 3). While the alloys undergo the fcc to hcp transformation on the first cycle, the transformation is suppressed or strongly shifted to lower temperatures on the second cycle. This behavior, which can be in principle attributed to a combination of transformation-related crystalline defects generation and the effect of the antiferromagnetic ordering, will be the subject of further research. Finally, a transition behavior is found if M_s is closer to T_N.

Acknowledgments

The authors gratefully acknowledge Dr. M.A. Arribere for performing the neutron activation chemical analyses of samples. Quartz capsules were prepared by Mr. E. Aburto and Mr. M.J. Isla. Research funding was provided by ANPCyT, Argentina (PICT 2012-0884), CONICET, Argentina (PIP 2011-0056) and U.N. Cuyo (06/C516).

References

[1] T. Maki, Ferrous shape memory alloys, in: K. Otsuka, C.M. Wayman (Eds.), Shape Memory Materials, Cambridge University Press, 1998.
[2] S. Cotes, M. Sade, A. Fernández Guillermet, Fcc/hcp martensitic transformation in the Fe-Mn system: experimental study and thermodynamic analysis of phase stabilities, Metall. Trans. 26A (1995) 1957–1969.
[3] P. Marinelli, A. Baruj, S. Cotes, A. Fernández Guillermet, M. Sade, The γ↔α' martensitic transformation in Fe-Mn and Fe-Mn-Co alloys: experiments, thermodynamic analysis and systematics of driving forces, Mater. Sci. Eng. A 273–275 (1999) 498–502.
[4] A. Nyilas, K. Weiss, G. Grikurov, N. Zoidze, Tensile, fracture, and fatigue crack growth rate behavior of high manganese steels, AIP Conf. Proc. 824 (I) (2006) 130–137.
[5] D.-S. Bae, S.-P. Lee, J.-K. Lee, U.-B. Baek, S.-H. Nahm, H. Takahashi, Effect of He-pre-injection on dislocation loop formation and irradiation-induced segregation of Fe–12%Cr–15%Mn austenitic steel, Fusion Eng. Des. 87 (2012) 1025–1029.
[6] P. Libeyre, D. Bessette, A. Devred, C. Jong, N. Mitchell, S. Sgobba, Conductor jacket development to meet mechanical requirement of the ITER central solenoid coils, Fusion Eng. Des. 86 (2011) 1553–1557.
[7] V. Mertinger, E. Nagy, M. Benke, F. Tranta, Characteristics of martensitic transformations induced by uni-axial tensile tests in a FeMnCr steel, Mater. Sci. Forum 812 (2015) 161–166.
[8] H.E. Troiani, M. Sade, G. Bertolino, A. Baruj, Martensitic transformation temperatures and microstructural features of FeMnCr alloys, Proc. Esomat 2009 2009, p. 06002.
[9] V. Mertinger, M. Benke, E. Nagy, T. Pataki, Reversible characteristics and cycling effects of the martensitic transformations in Fe-Mn-Cr TWIP/TRIP steels, J. Mater. Eng. Perform. 23 (2014) 2347–2350.
[10] Y. Watanabe, H. Sato, Y. Nishino, I. Kim, Training effects on damping capacity in Fe-Mn and Fe-Mn-Cr alloys, Mater. Sci. Forum 638–642 (2010) 2201–2206.
[11] O. Grässel, L. Krüger, G. Frommeyer, L.W. Meyer, High strength Fe-Mn-(Al, Si) TRIP/TWIP steels development - properties - application, Int. J. Plast. 16 (2000) 1391–1409.
[12] I. Nikulin, T. Sawaguchi, K. Tsuzaki, Effect of alloying composition on low-cycle fatigue properties and microstructure of Fe-30Mn-(6x)*Si*-xAl TRIP/TWIP alloys, Mater. Sci. Eng. A 587 (2013) 192–200.
[13] J. Millán, S. Sandlobes, A. Al-Zubi, T. Hickel, P. Choi, J. Neugebauer, D. Ponge, D. Raabe, Designing Heusler nanoprecipitates by elastic misfit stabilization in Fe-Mn maraging steels, Acta Mater. 76 (2014) 94–105.
[14] A. Cladera, B. Weber, C. Leinenbach, C. Czaderski, M. Shahverdi, M. Motavalli, Iron-based shape memory alloys for civil engineering structures: an overview, Constr. Build. Mater. 63 (2014) 281–293.
[15] T. Sawaguchi, P. Sahu, T. Kikuchi, K. Ogawa, S. Kajiwara, A. Kushibe, M. Higashino, T. Ogawa, Vibration mitigation by the reversible fcc/hcp martensitic transformation during cyclic tension compression loading of an Fe-Mn-Si-based shape memory alloy, Scr. Mater. 54 (2006) 1885–1890.
[16] T. Sawaguchi, L.-G. Bujoreanu, T. Kikuchi, K. Ogawa, M. Koyama, M. Murakami, Mechanism of reversible transformation-induced plasticity of Fe-Mn-Si shape memory alloys, Scr. Mater. 59 (2008) 826–829.
[17] T. Sawaguchi, I. Nikulin, K. Ogawa, K. Sekido, S. Takamori, T. Maruyama, Y. Chiba, A. Kushibe, Y. Inouec, K. Tsuzaki, Designing Fe–Mn–Si alloys with improved low-cycle fatigue lives, Scr. Mater. 99 (2015) 49–52.
[18] V. Mertinger, M. Benke, E. Nagy, Effect of Cr content on the TWIP behavior in Fe-Mn-Cr steels, Mater. Today: Proc. 2 (2015) S673–S676.
[19] O.A. Khomenko, I.F. Khil'kevich, G.Y. Zvigintseva, Influence of a third component on the Néel point of iron-manganese invars, Fiz. Met. Metalloved. 37 (1974) 1325–1326.
[20] Y.S. Zhang, X. Lu, X. Tian, Z. Quin, Compositional dependence of the Néel transition, structural stability, magnetic properties and electrical resistivity in Fe-Mn-Al-Cr-Si alloys, Mater. Sci. Eng. A 334 (2002) 19–27.
[21] M. Sade, A. Baruj, H.E. Troiani, fcc/hcp martensitic transformation temperatures and thermal cycling evolution in Fe-Mn-Cr alloys, Proc. Int. Conf. New Developments on Metallurgy and Applications of High Strength Steels, Buenos Aires, Argentina 2008, pp. 1183–1191.
[22] S. Cotes, A. Fernández Guillermet, M. Sade, Phase stability and fcc/hcp martensitic transformation in Fe-Mn-Si alloys. Part I. Experimental study and systematics of the M_s and A_s temperatures, J. Alloys Compd. 278 (1998) 231–238.
[23] A. Baruj, S. Cotes, M. Sade, A. Fernández Guillermet, Coupling binary and ternary information in assessing the fcc/hcp relative phase stability and martensitic transformation in Fe-Mn-Co and Fe-Mn-Si alloys, J. Phys. IV France 5 (1995) (C8-373-378).
[24] J.B. Sousa, M.R. Chaves, M.E. Braga, M.M. Reis, M.F. Pinheiros, M. Crisan, Critical behaviour of the electrical resistivity near the Néel point in antiferromagnetic Cr-Mn alloys, J. Phys. F 5 (1975) L155–L158.
[25] S. Arajs, K.B. Rao, H.U. Astrom, F. De Young, Determination of Néel temperatures of binary chromium alloys from electrical resistivity data, Phys. Scr. 8 (1973) 109–112.
[26] S. Eucken (Ed.), Progress in Shape Memory Alloys, DGM Informationgesellschaft, Germany, 1992.
[27] A. Baruj, Martensitic Transformation, fcc and hcp Relative Phase Stability, and Thermal Cycling Effects in Fe-Mn and Fe-Mn-X Alloys (X = Si, Co), Instituto Balseiro, U.N. Cuyo, Argentina, 1999 (pH.D. Thesis, in Spanish).
[28] W. Huang, An assessment of the Fe-Mn system, Calphad 13 (1989) 243–252.
[29] A. Baruj, A. Fernández Guillermet, M. Sade, The fcc/hcp relative phase stability in the Fe-Mn-Co system: martensitic transformation temperatures, assessment of Gibbs energies and thermodynamic calculation of T_0 lines, J. Phys. IV France 7 (1997) (C5-405-410).
[30] S.M. Cotes, A. Fernández Guillermet, M. Sade, Fcc/hcp martensitic transformation in the Fe-Mn system: part II. Driving force and thermodynamics of the nucleation process, Metall. Mater. Trans. A 35A (2004) 83–91.